Supporting Information

Schneider et al. 10.1073/pnas.1305378110

SI Text

Proteros Reporter Displacement Assay. In brief, the assay (1, 2) is based on the competitive displacement of a reporter probe designed to selectively target the cyclin-dependent kinase 8 (CDK8) ATP binding site with a fast binding kinetic signature. Binding of the probe to its target results in the emission of an optical signal. Competitive displacement of the probe by the corresponding compounds (fragment or lead-like type) results in a loss of the optical signal that can be quantified with increasing compound concentrations. The half-inhibitory concentration (IC_{50}) measurement of the library screen was quantified by regular IC_{50} fitting of the percent reporter displacement values (with no displacement of the reporter corresponding to 0% and complete displacement corresponding to 100% after 15 and 80 min). With the previously determined K_d value of the reporter and its known concentration, the K_d value of the compound is then calculated within the equilibrated system from the measured IC_{50} value by the Cheng–Prusoff equation (Eq. **S1**):

$$K_d(\text{compound}) = IC_{50}/(1 + [\text{reporter}]/K_d(\text{reporter})), \quad \textbf{[S1]}$$

where K_d(compound) is the dissociation constant of the corresponding compound, IC_{50} is the concentration at which 50% of reporter binding is displaced, [reporter] is the known concentration of the reporter probe, and K_d(reporter) is the value of the previously determined dissociation constant of the reporter probe (in this case: 142.4 nM).

Binding kinetics was analyzed by fitting the reporter displacement traces for individual compound concentrations to a monoexponential decay equation. Thereby an exponent is yielded that reflects the observed association rate k_{obs} for each concentration. Then each k_{obs} value is plotted on the y axis against the corresponding compound concentrations (x axis) and fitted to linear Eq. **S2**:

$$k_{obs} = k_{off} + k_{on} \times [\text{compound}], \quad \textbf{[S2]}$$

where k_{obs} is the observed association rate, k_{off} is the dissociation rate constant, k_{on} is the association rate constant, and [compound] is the compound concentration. Thus, k_{on} is obtained from the slope.

The k_{off} rate then is obtained by Eq. **S3**:

$$k_{off} = k_{on} \times K_d, \quad \textbf{[S3]}$$

where k_{off} is the dissociation rate, k_{on} is the association rate, and K_d is the dissociation constant.

The residence time is calculated from the dissociation rate in Eq. **S4**:

$$\text{residence time} = 1/k_{off}. \quad \textbf{[S4]}$$

To assure that the k_{obs} value reflects only the compound binding and not the probe dissociation, a probe with a fast dissociation rate (high k_{off} value) was used. Thus, in all cases the rate-limiting step is not probe dissociation but compound binding.

In Table S2, error estimation and correlation coefficients for the binding kinetics are shown.

Time-Resolved IC_{50} Determination of Hit Compounds of the Primary Screen. Two hundred and ten hit compounds of the primary screen (hit rates, Table S1), which comprised fragments and lead-likes of different compound classes, were selected for time-resolved IC_{50} determination. As compounds with long residence time capacities ($1/k_{off}$, Eq. **S4**) are characterized by the dissociation rate (small k_{off} value), the IC_{50} values were measured 15 and 80 min after compound addition to the probe–target complex. Compounds with slow binding kinetics [small observed association rate constant (k_{obs}) values, Eq. **S2**] are characterized by having a smaller IC_{50} value after 80 min compared with 15 min. Because the rate of reaching the equilibrium IC_{50} value is given by the value of k_{obs} (Eq. **S2**), and because k_{obs} depends on the k_{off} value, compounds with a time-dependent IC_{50} value are likely to show slow (small) k_{off} rates which define in their reciprocal values long residence time values. In Fig. S1 the corresponding IC_{50} values were plotted with the value for 15 min on the x axis and the value for 80 min on the y axis. Compounds with fast binding kinetics (residence time below the detection limit <1.4 min up to <15 min due to the experimental protocol) are located on the bisecting line, whereas compounds with slow binding kinetics (residence time >15 min) are located below.

Detailed Binding Mode of the Compounds of the Structure–Kinetic Relationship Series in Complex with Human CDK8/Cyclin C. For a better overview, the CDK8 residues within the active site were assigned to the specific pockets and kinase regions as follows: (*i*) deep pocket and interacting residues (Ser62, Arg65, Leu70, Leu73, Val78, Leu142, His149; forest green), (*ii*) "key" residues of the DMG motif and kinome-wide conserved salt bridge (Asp173, Met174, Glu66, Lys52; gold), (*iii*) DMG-motif surrounding residues (Ile171, Ala172, Gly175, Phe176, Ile79, Phe97; pea green), (*iv*) β1–β2 loop residues (Val27, Tyr32, Val35, Ala50; purple), (*v*) hinge residues (Asp98, Tyr99, Ala100, Glu101; turquoise), and (*vi*) front pocket residues and its surrounding (Trp105, His106, Ala155, Leu158, Arg356; marine blue).

The deep pocket binding moiety of the minimal compound 7 (Fig. S3*A*) is anchored within the deep pocket (forest green) and forms hydrophobic contacts with neighboring residues of the DMG motif (gold), its surroundings (pea green), and $Tyr32^{CDK8}$ (purple, β1–β2 loop). The urea linker forms H bonds with $Glu66^{CDK8}$ (gold, αC helix) and the $Asp173^{CDK8}$ main-chain amide (gold, DMG motif), but does not disrupt the salt bridge of the kinome-wide conserved $Glu66^{CDK8}$–$Lys52^{CDK8}$ ion pair. Compound 3 (Fig. S3*B*) is found in a similar binding mode, including only a few more hydrophobic contacts. The terminal hydroxyl group of its hinge-directed moiety is found within H-bonding distance of $Lys52^{CDK8}$, but H bonding may be weak due to a disadvantageous angle. Analogously, the terminal (2-morpholine-4-yl)ethyl-group of compound 4 (Fig. S3*C*) cannot contact the hinge region and displaces the position of the $Tyr32^{CDK8}$ side chain out from the β1 sheet. Consequently, the side chain of $Met174^{CDK8}$ is shifted even further out of the active site, leaving Gly175-$Phe176^{CDK8}$ disordered. The main-chain carbonyl of $Asp173^{CDK8}$ appears in H-bonding distance of the nitrogen of the pyrazole ring but due to an unfavorable angle it rather forms a H bond with $Glu66^{CDK8}$. The additional methyl group in the hinge-directed moiety of compound 5 enables hinge interaction by the terminal (3-morpholine-4-yl)propyl group via H bonding ($Ala100^{CDK8}$ backbone-amide; Fig. S3*D*, turquoise). Interestingly, $Tyr32^{CDK8}$ exhibits the same orientation as in the complex with the compounds 7 and 3 (Fig. S3 *A* and *B*) and interacts with the compound 5 deep pocket binding moiety. Compared with compound 4, further van der Waals contacts are established between the terminal morpholine moiety of compound 5 with the β1–β2 loop and the

DMG-motif surroundings. The high resolution (2.1 Å) of this X-ray structure reveals the presence of a water molecule that enables H bonding between the pyrazole ring of the deep pocket binding moiety and $Arg65^{CDK8}$. The orientation of $Arg65^{CDK8}$ is similar for all structures and indicates that this water molecule should be present overall. Compound 11 (Fig. S3*E*) forms a second H bond with the hinge region ($Asp98^{CDK8}$ backbone carbonyl; $Ala100^{CDK8}$ backbone amide). In contrast, compound 2 forms the three standard H bonds but does not contact the hinge region at all (Fig. S3*F*). A slight variation positions the main-chain amide of $Asp173^{CDK8}$ in H-bonding distance of the urea linker of compound 2 but the unfavorable angle does not allow for H-bond formation. The tertiary butyl of compound 2 is stabilized in a van der Waals distance of $Arg356^{CDK8}$ that gets involved in this front pocket interaction (marine blue). Similarly, the hinge-directed moiety of compound 1 (Fig. S3*G*) does not interact with the hinge region. Its piperazine ring forms hydrophobic contacts with $Tyr32^{CDK8}$, which adopts a similar conformation as observed for the complex with compound 4 (Fig. S3*C*). The terminal moiety of compound 1 forms extensive contacts within the front pocket ($Arg356^{CDK8}$ π-stacking with the tolyl moiety), which are completed by interactions with $His106^{CDK8}$ and $Trp105^{CDK8}$ (αD helix/C lobe). Due to the resolution of this structure (2.4 Å), additional H-bond bridging water molecules are found, involving $Tyr32^{CDK8}$ and $Asn165^{CDK8}$ ("η1"-3_{10}helix/C lobe).

Interactions of Compounds in Relation to Their Residence Time. The number of contacts within the binding surface with the SKR compound was analyzed for each interacting atom of CDK8/CycC (cyclin C) (Table S5). Besides the sum of H bonds, hydrophobic contacts were calculated per atom (carbons, sulfur, and halogens) using the sum of the van der Waals radii + 0.5 Å (contact atoms as defined by Lo Conte et al., ref. 3) that we varied by ±0.2 Å to respect rmsd differences and kinase dynamics of the different CDK8/CycC crystal structures [resolution 2.1–3.0 Å; calculations performed with CCP4 (ref. 4), structure analysis]. In the case of π-stacking every atom was counted, in agreement with the electrochemical properties of this interaction. H-bond formation involving water molecules was not considered due to experimental uncertainties at low resolution (3).

Superposition of the Compounds of the SKR Series. Even though the overlay was centered on CDK8, the central urea linker and the deep pocket binding moiety of all SKR compounds align closely, whereas their hinge-directed moieties differ in orientation and position (Fig. S4).

CDK8/CycC DMG-In Conformation. An extensive CDK8 T-loop/CycC interaction is observed in the CDK8/CycC apo form (Fig. S5*A*, DMG-in conformation with the CDK8 T-loop segment defined including residue 184), which is disordered in all other CDK8/CycC SKR-compound complexes (CDK8 T-loop segment disorder starting at least with residue 178). This observation appears of high importance because no activatory phosphorylation of the CDK8 T-loop has been observed yet in contrast with the general mechanism of CDK activation (5, 6). Based on the comprehensive structural information on CDK2 structures, it was discovered that the general CDK activation process requires two steps including binding of the cyclin to rearrange the CDK αC helix toward the activation segment and reversible phosphorylation of the CDK T-loop: subsequently, an electrostatic network with a conserved arginine triade interacts with the phosphor residue to maintain the activation segment in an open conformation. However, several crystal structures have already questioned the universal validity of this two-step activation model such as CDK4/CycD (7, 8). In the absence of a phosphorylated T loop as an anchor point, the T loop observed in the CDK8/CycC apo structure is positioned within an extensive H-bond network with CycC (Fig. S5*A*). The activation of CDK8 by CycC based on a phosphorylated-residue–mimicking residue of CycC ($Glu99^{CycC}$) has been discussed previously (9). In fact, we observed that the CycC H3–H4 loop is in a relaxed position and shifted toward CDK8 to position $Glu99^{CycC}$ appropriately. Two of the three conserved arginines of CDK8 ($Arg65^{CDK8}$ and $Arg150^{CDK8}$) contact the exposed side chain of $Glu99^{CycC}$ and the $Val97^{CycC}$ backbone carbonyl via H bonding. Just too distant of the CycC binding surface the main-chain carbonyl of the third conserved arginine, $Arg178^{CDK8}$, interacts with the main-chain carbonyl of $Asn181^{CDK8}$. This interaction obviously serves as another anchor to position the CDK8 T loop, which is strengthened by H bonding between the $Glu99^{CycC}$ main-chain carbonyl with the $Phe180^{CDK8}$ main-chain amide. Similarly, it was reported for CDK2 (Fig. S5*B*) that a glutamate ($Glu162^{CDK2}$) can compensate the lack of the phosphate group at the CDK2 T loop: the CDK2 T loop is found within an at least partially active conformation that allows a correct positioning of ATP but limits the CDK2 kinase activity to 1% (5, 10). Moreover, a phosphorylation-independent kinase activation has been observed for the CDK6 kinase by complex formation with the virus-encoded cyclin of Herpesvirus saimiri. In this complex, the open conformation segment of CDK6 is described as similar to the phosphorylated and fully active CDK2 complex (11).

1. Neumann L, Ritscher A, Müller G, Hafenbradl D (2009) Fragment-based lead generation: Identification of seed fragments by a highly efficient fragment screening technology. *J Comput Aided Mol Des* 23(8):501–511.
2. Neumann L, von König K, Ullmann D (2011) HTS reporter displacement assay for fragment screening and fragment evolution toward leads with optimized binding kinetics, binding selectivity, and thermodynamic signature. *Methods Enzymol* 493:299–320.
3. Lo Conte L, Chothia C, Janin J (1999) The atomic structure of protein-protein recognition sites. *J Mol Biol* 285(5):2177–2198.
4. Dodson EJ, Winn M, Ralph A (1997) Collaborative Computational Project, number 4: providing programs for protein crystallography. *Methods Enzymol* 277:620–633.
5. Jeffrey PD, et al. (1995) Mechanism of CDK activation revealed by the structure of a cyclinA-CDK2 complex. *Nature* 376(6538):313–320.
6. Pavletich NP (1999) Mechanisms of cyclin-dependent kinase regulation: Structures of Cdks, their cyclin activators, and Cip and INK4 inhibitors. *J Mol Biol* 287(5):821–828.
7. Day PJ, et al. (2009) Crystal structure of human CDK4 in complex with a D-type cyclin. *Proc Natl Acad Sci USA* 106(11):4166–4170.
8. Takaki T, et al. (2009) The structure of CDK4/cyclin D3 has implications for models of CDK activation. *Proc Natl Acad Sci USA* 106(11):4171–4176.
9. Hoeppner S, Baumli S, Cramer P (2005) Structure of the mediator subunit cyclin C and its implications for CDK8 function. *J Mol Biol* 350(5):833–842.
10. Noble M, et al. (2005) Exploiting structural principles to design cyclin-dependent kinase inhibitors. *Biochim Biophys Acta* 1754(1-2):58–64.
11. Schulze-Gahmen U, Kim SH (2002) Structural basis for CDK6 activation by a virus-encoded cyclin. *Nat Struct Biol* 9(3):177–181.

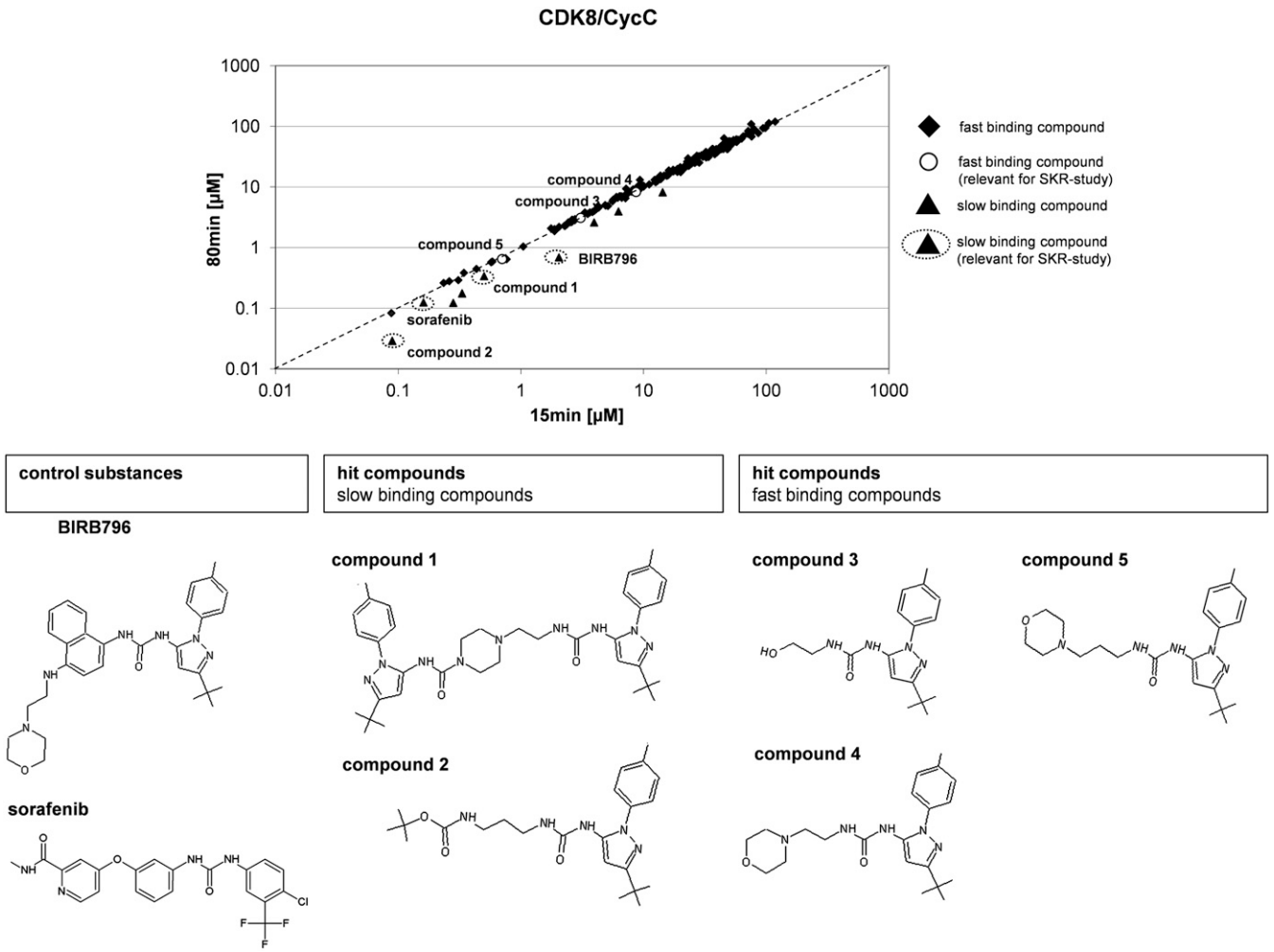

Fig. S1. IC_{50} determination of selected hit compounds of the primary screen.

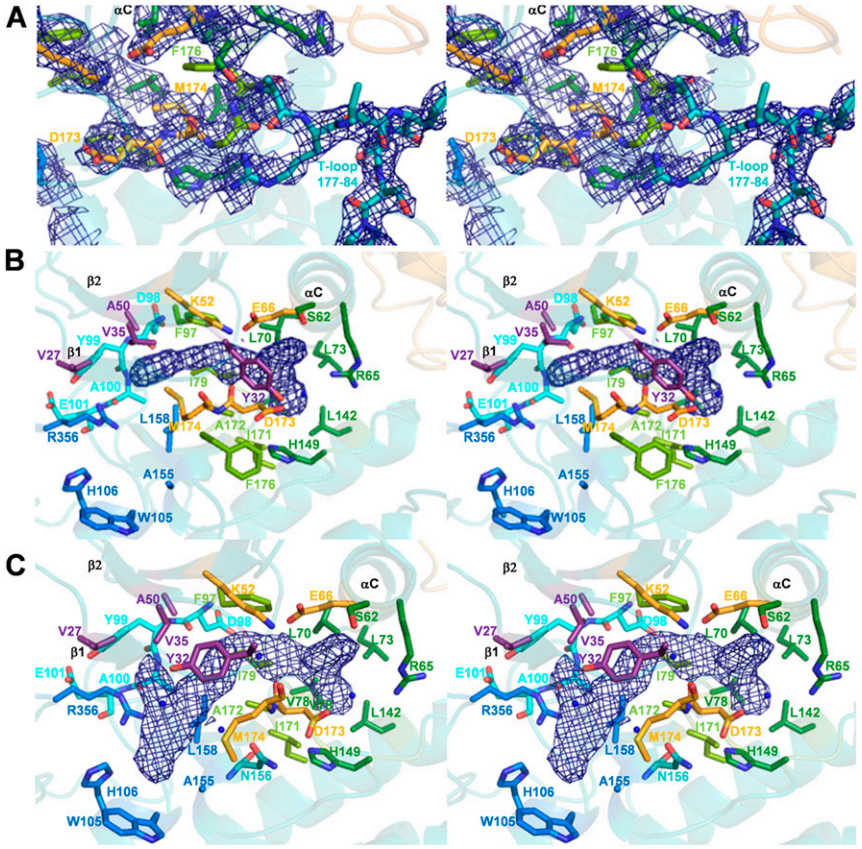

Fig. S2. Comparison of the activation segment of CDK8/CycC. CDK8 (teal)/CycC (gold); CDK8 residues are assigned to distinctive parts of the kinase (teal) and shown as sticks with the carbons colored as follows: conserved residues in interaction with type II compounds (gold), DMG-motif surrounding residues (pea green), deep pocket located and surrounding residues (forest green), β1–β2 sheet residues (purple), hinge-region residues (turquoise), and front pocket residues (marine blue). Other atoms are colored according to atom type: nitrogen (blue), oxygen (red), sulfur (saffron). Water molecules are indicated as blue nonbound spheres. (*A*) CDK8/CycC apo form in the DMG-in conformation (4G6L); $Tyr32^{CDK8}$ side chain is disordered; the residues of the active site are shown superimposed with the refined 2Fo-Fc electron density map (density blue) contoured at 1σ, which was calculated from the final model after residues of the DMG-motif, T-loop, and Glu–Lys ion bridge (173–184; 52, and 66) had been omitted; residues of the CDK8 T-loop, which are only defined within the DMG-in conformation, are shown as sticks (177–184; teal); the weak density of $Phe176^{CDK8}$ within the 2Fo-Fc omit map indicates its flexibility. (*B* and *C*) Refined 2Fo–Fc omit maps (density blue) of SKR compounds; these were calculated from the final models after compounds 1and 5 had been omitted and are contoured at 1σ; (*B*) CDK8/CycC/compound 5 complex in the DMG-out-conformation; (*C*) CDK8/CycC/compound 1 complex in the DMG-out conformation.

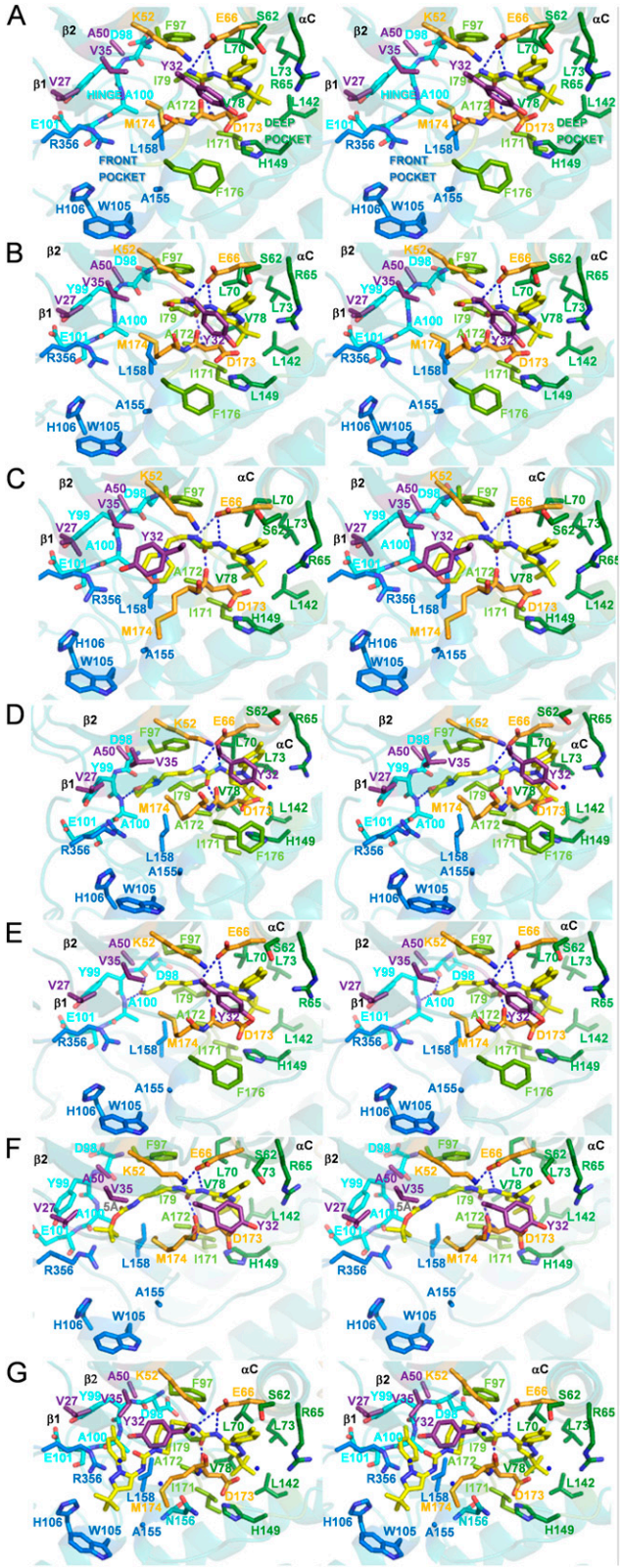

Fig. S3. Detailed binding mode of the compounds of the SKR series in complex with human CDK8/CycC. The CDK8 residues are colored according to the specific parts of the kinase as described in the text. Compounds are shown as sticks with their carbons colored yellow. Heteroatoms are colored according to atom type: nitrogen (blue), oxygen (red), sulfur (saffron). In general, H bonds are indicated for compound-CDK8 interaction (blue dotted lines) and H bonds bridging water molecules as blue nonbound spheres. CycC is not shown for clarity. Secondary structural elements are labeled black. All close-up stereo figures were positioned to allow best view depending on the inhibitor's binding mode to CDK8/CycC; *A*) compound 7 (SRTC, <1.4 min); disordered activation segment residues 178–194; *B*) compound 3 (SRTC, <1.4 min); disordered activation segment residues 177–194; *C*) compound 4 (SRTC, <1.4 min); disordered activation segment: residues 175–194; *D*) compound 5 with a detectable residence time (14 min); disordered activation segment residues 177–193; *E*) compound 11 (LRTC,

Legend continued on following page

57 min); disordered activation segment residues 177–193; *F*) compound 2 (LRTC, 1,944 min); gray label indicates distance to hinge region; disordered activation segment residues 176–195 and Tyr32^{CDK8}; *G*) compound 1 (LRTC, 1,626 min); additional hydrophilic interactions are bridged by water molecules involving Tyr32^{CDK8} and Asn156^{CDK8} (teal); disordered activation segment residues: 176–195. LRTC, compounds with long residence times; SRTC, compounds with short residence times.

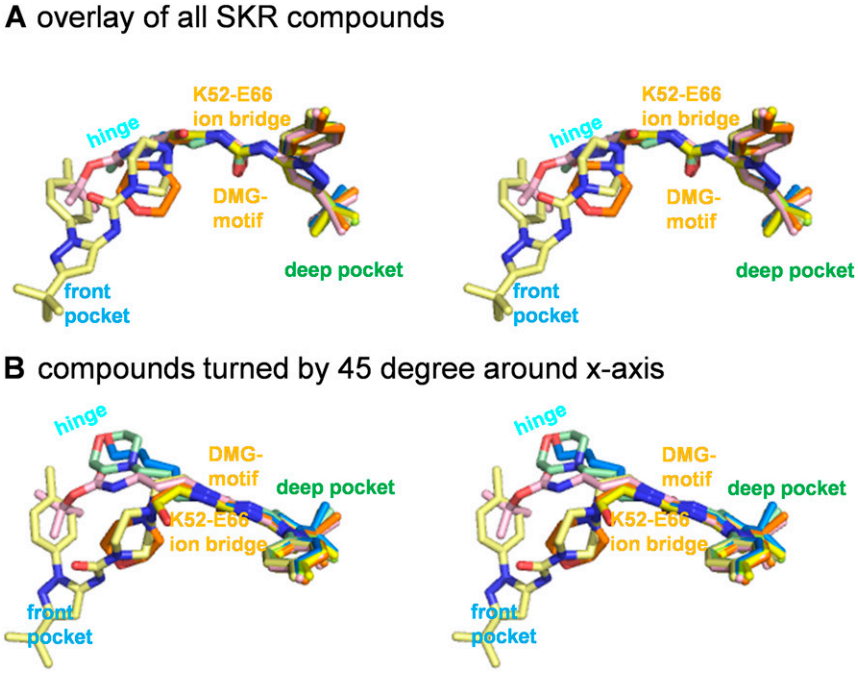

Fig. S4. Overlay of the SKR compounds (*A*) and turned by 45 degree around x-axis (*B*). The overlay is centered on CDK8 of CDK8/CycC in complex with the minimal compound 7 (4F6S) using COOT/"Secondary-structure matching (SSM)" (1): CDK8/CycC in complex with: compound 3 (4F7J): rmsd 0.4A; compound 4 (4F70): rmsd 0.3A; compound 5 (4F6U): rmsd 0.4 A; compound 2 (4F7L): rmsd 0.4A; compound 1 (4F6W): rmsd 0.4A; compound 11 (4F7N): rmsd 0.3A; all X-ray structures share a sequence identity of 100%. The compounds are shown as sticks with atoms colored according to atom type: nitrogen (blue), oxygen (red), carbon according to compound identity as follows: compound 7 (carbon: lemon), compound 3 (carbon: yellow), compound 4 (carbon: orange), compound 5 (carbon: pale green), compound 11 (carbon: marine blue), compound 2 (carbon: rose) and compound 1 (carbon: pale yellow). For clarity, CDK8/CycC residues were omitted and only important kinase-parts are indicated with labels.

1. Krissinel E, Henrick K (2004) Secondary-structure matching (SSM), a new tool for fast protein structure alignment in three dimensions. *Acta Crystallogr D Biol Crystallogr* 60(Pt12 Pt 1): 2256–2268.

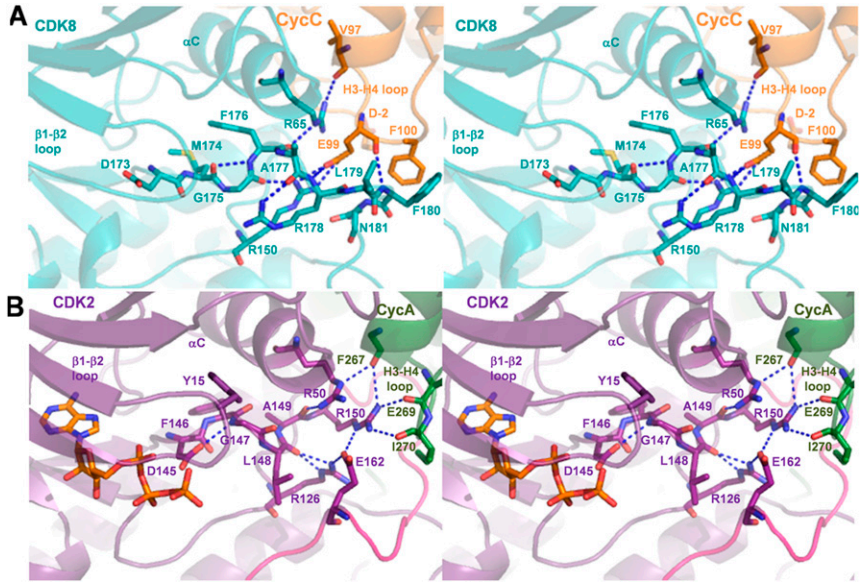

Fig. S5. Comparison of the activation segment of CDK8/CycC and CDK2/CycA. Atoms are colored according to atom type: nitrogen (blue), oxygen (red), sulfur (saffron). (*A*) CDK8 (teal)/CycC (gold) interaction surface based on the CDK8 T loop. H bonding is indicated with blue dotted lines. (*B*) Close-up of the unphosphorylated activation segment of the CDK2 (plum)/CycA (forest green)/ATP (deep orange) complex (1FIN); H bonds are indicated as blue dotted lines in accordance with Kornev et al. (1) For further details see the text.

1. Kornev AP, Haste NM, Taylor SS, Eyck LF (2006) Surface comparison of active and inactive protein kinases identifies a conserved activation mechanism. *Proc Natl Acad Sci USA* 103(47): 17783–17788.

Table S1. Results of the primary screen

	Lead-like	Hit rate, %	Fragment	Hit rate, %
Tested compounds	2,729		2,192	
Maximal assay concentration	1.91 μM		38.2 μM	
Inhibition ≥ 70%	68	2.5	286	13.0
Inhibition ≥ 80%	52	1.9	201	9.2
Inhibition ≥ 90%	39	1.4	136	6.3

Table S2. Error estimation of the binding kinetics of the SKR compounds

Compound ID	IC50, μM; std error IC_{50}, μM	Hill std error Hill	r^2 IC_{50}	K_d, μM; error K_d, μM	k_{on}, , $s^{-1}{\cdot}\mu M^{-1}$; std error k_{on} , $s^{-1}{\cdot}\mu M^{-1}$	r^2 secondary plot	k_{off}, s^{-1}; error k_{off}, s^{-1}	Residence time, min; error residence time, min	Replicates
6	>934	—	—	—	—	—	—	—	3
7	6.47	0.76	0.98	3.24	—	—	—	—	3
	1.52	0.10		0.76					
8	3.14	1.01	0.98	1.57	—	—	—	—	3
	0.56	0.15		0.28					
3	11.6	0.70	0.96	5.82	—	—	—	—	3
	1.75	0.07		0.88					
4	3.64	0.89	0.97	1.82	—	—	—	—	3
	0.39	0.08		0.20					
9	7.06	0.76	0.99	3.53	—	—	—	—	3
	0.77	0.05		0.39					
10	2.60	1.05	0.96	1.30	1.85×10^{-3}	0.97	2.41×10^{-3}	7	3
	0.49	0.18		0.24	2.10×10^{-4}		5.31×10^{-4}	2	
5	1.41	1.77	0.95	0.70	1.68×10^{-3}	0.99	1.18×10^{-3}	14	3
	0.19	0.37		0.10	7.28×10^{-5}		1.70×10^{-4}	2	
11	0.16	0.99	0.99	0.08	3.65×10^{-3}	0.97	2.90×10^{-4}	57	3
	0.02	0.09		0.01	3.58×10^{-4}		4.28×10^{-5}	8	
2	0.03	1.19	0.99	0.01	5.73×10^{-4}	0.99	8.57×10^{-6}	1,944	3
	0.003	0.12		0.001	2.69×10^{-5}		9.25×10^{-7}	210	
1	0.07	1.29	0.99	0.03	2.99×10^{-4}	0.99	1.02×10^{-5}	1,626	3
	0.006	0.12		0.003	1.62×10^{-5}		1.03×10^{-6}	164	
Type I	4.88	0.89	0.99	2.44	—	—	—	—	3
Compound	0.78	0.10		0.39					

SE (std error): based on fitting performance. Error K_d [μM]: $SE(IC_{50})/2$ according to Gaussian error propagation. Error k_{off} [1/s]: $((K_d \times SE(k_{on}))^2 + (k_{on} \times SE(K_d)^2)^{0.5}$ according to Gaussian error propagation. Error residence time [min]: $= (SE(k_{off})/(k_{off})^2)/60$.

Table S3. Data collection and processing statistics

Compound	7 (4F6S)	3 (4F7J)	4 (4F70)	5 (4F6U)	11 (4F7N)	2 (4F7L)	1 (4F6W)	apo (4G6L)	4F7S
X-ray source	PXI/X06SA (SLS)*								
Detector	PILATUS 6M								
Space group	$P\ 2_1\ 2_12_1$	$P\ 2_1\ 2_1\ 2_1$	$P\ 2_1\ 2_1\ 2_1$	$P\ 2_1\ 2_1\ 2_1$	$P\ 2_1\ 2_1\ 2_1$	$P\ 2_1\ 2_1\ 2_1$	$P\ 2_1\ 2_1\ 2_1$	$P\ 2_1\ 2_1\ 2_1$	$P\ 2_1\ 2_1\ 2_1$
Cell, Å									
a	71.04	71.53	71.49	71.40	72.16	71.82	71.12	70.18	70.50
b	71.39	71.91	71.85	71.02	71.76	71.24	71.71	70.94	70.77
c	171.72	176.90	171.04	171.22	180.36	171.71	171.87	170.42	170.14
α, °	90.0	90.0	90.0	90.0	90.0	90.0	90.0	90	90
β, °	90.0	90.0	90.0	90.0	90.0	90.0	90.0	90	90
γ, °	90.0	90.0	90.0	90.0	90.0	90.0	90.0	90	90
Resolution, Å	2.60	2.60	3.00	2.10	2.65	2.90	2.39	2.70	2.20
	(2.81–2.60)	(2.81–2.60)	(3.24–3.00)	(2.27–2.10)	(2.86–2.65)	(3.09–2.90)	(2.58–2.39)	(2.87–2.70)	(2.34–2.20)
Unique reflections	27,589	28,771	18,292	51,626	27,863	19,174	35,593	24,071	43,856
	(5505)	(5,832)	(3673)	(10,340)	(5,620)	(2,853)	(7,102)	(4,009)	(7,387)
Multiplicity	8.1 (8.4)	5.4 (5.5)	8.0 (8.3)	8.1(8.0)	3.7 (3.7)	3.9 (3.3)	8.1 (8.1)	8.1 (8.3)	5.4 (5.6)
Completeness, %	99.9 (99.7)	99.7 (99.4)	99.9 (99.7)	99.9 (100.0)	99.7 (99.6)	94.9 (84.3)	100.0 (100.0)	99.9 (99.7)	99.5 (99.5)
R_{sym}, %†	9.3 (63.5)	9.0 (50.4)	11.4 (51.1)	6.5 (54.9)	7.6 (51.5)	8.1 (43.2)	8.2 (59.4)	12.1 (67.9)	7.4 (68.3)
R_{meas}, %‡	10.0 (67.7)	10.8 (61.2)	13.0 (58.2)	7.0 (58.7)	10.3 (68.7)	9.3 (50.9)	8.7 (63.5)	12.9 (72.3)	8.1 (75.5)
Mean(I)/SD	17.83 (4.54)	10.6 (2.5)	13.1 (4.1)	20.87 (4.43)	9.2 (2.0)	14.22 (3.29)	19.08 (4.30)	15.62 (3.54)	15.60 (2.76)

*Swiss Light Source (SLS, Villigen, Switzerland).
†Values in parentheses refer to the highest resolution bin.
‡Calculated from independent reflections.

Table S4. Refinement statistics

Compound	7 (4F6S)	3 (4F7J)	4 (4F70)	5 (4F6U)	11 (4F7N)	2 (4F7L)	1 (4F6W)	apo (4G6L)	4F7S
Resolution, Å	85.86–2.60	88.45–2.60	85.52–3.00	85.61–2.10	90.19–2.65	85.85–2.90	85.94–2.39	85.21–2.70	85.07–2.20
Number of reflections (working/test)	26,652/936	27,752/958	17,610/630	49,911/1715	26,899/908	18,512/662	34,411/1181	23,226/844	42,388/1,468
R_{cryst}, %	20.4	22.8	20.3	17.6	19.9	22.4	19.2	21.2	19.3
R_{free}, %	26.2	27.6	23.9	19.8	22.8	27.0	23.4	26.2	22.2
Test set (amount of measured reflections), %	3.4	3.3	3.5	3.3	3.3	3.5	3.3	3.5	3.3
Total no. of atoms									
Protein	4,925	4,945	4,919	4,994	4,993	4,928	4,951	5,004	5,036
Water	90	58	32	309	61	25	150	40	209
Ligand	20	23	28	29	26	31	47	—	19
Deviation from ideal geometry									
Bond lengths, Å	0.009	0.010	0.009	0.010	0.009	0.011	0.011	0.010	0.010
Bond angles, °	1.17	1.23	1.09	1.21	1.18	1.28	1.27	1.21	1.18
Bonded B's, Å	3.0	2.8	1.3	2.8	1.7	2.6	3.5	2.8	2.6
Ramachandran plot:									
Most favored regions, %	93.8	92.1	92.7	93.3	94.6	90.1	94.4	92.8	94.3
Additional allowed regions, %	6.2	7.5	7.1	6.7	5.4	9.5	5.6	7.0	5.7
Generously allowed regions, %	0.0	0.4	0.2	0.0	0.0	0.4	0.0	0.2	0.0
Disallowed regions, %	0.0	0.0	0.0	0.0	0.0	0.0	0.0	0.0	0.0

The final models, which comprise residues for CDK8 and CycC according to the sequence in Swiss-Prot ID P49336 and P24863, and their completeness, as defined by electron density, are listed in the following. Additional residues were introduced (termed -1, 0, where 1 refers to $Met1^{CDK8}$ and -3, -2, -1, 0 where 1 refers to $Met1^{CycC}$) at the N terminus of each protein during cloning at the cleavage site. CDK8/CycC in complex with compound: 7 (4F6S): chain A (CDK8 residues 0–359) except for the segments 115–122, 178–194, 238–244, and 360–403; chain B (CycC residues −1–264) except for the segment 265–283; 3 (4F7J): chain A (CDK8 residues 1–359) except for the segments 113–121, 177–194, 239–244, and 360–403; chain B (CycC residues −3–264) except for the segment 265–283; 4 (4F70): chain A (CDK8 residues 0–359) except for the segments 117–122, 175–194, 238–244, and 360–403; chain B (CycC residues −1–264) except for the segments 265–283; 5 (4F6U): chain A (CDK8 residues −1–359) and chain B (CycC residues −2–264) except for the segments 116–120, 177–193, 240–244, and 360–403; 11 (4F7N): chain A(CDK8 residues 0–361) except for the segments 115–120, 177–193, 240–244, and 362–403; chain B (CycC residues −2–265) except for the segment 266–283; 2 (4F7L): chain A (CDK8 residues −1–359) except for the segments 115–121, 176–195, 239–244, and 360–403; chain B (CycC residues −1–264) except for the segment 265–283; 1 (4F6W): chain A (CDK8 residues 1–359) except for the segments 116–120, 178–195, 239–244, and 360–403; chain B (CycC residues 2–264) except for the segment 265–283; CDK8/CycC/apo (4G6L): chain A (CDK8 residues −2–359) except for the segments 115–122, 185–196, 240–245, and 360–403; chain B (CycC residues -2-264) except for the segment 265–283; 4F7S chain A (CDK8 residues −1–359) except for the segments 115–121, 176–195, 239–244, and 360–403; chain B (−1–264) except for the segment 265–283.

Table S5. Interactions of compounds in relation to their residence time

Compound ID (PDB-ID)	7 (4F6S)	3 (4F7J)	4 (4F70)	5 (4F6U)	11 (4F7N)	2 (4F7L)	1 (4F6W)
H bonds	3	3	3	4	5	3	3
Hydrophobic contacts	48 (30)	46 (33)	50 (30)	66 (48)	60 (41)	72 (46)	96 (66)
Sum of contacts	51 (33)	49 (36)	53 (32)	70 (52)	63 (44)	78 (51)	99 (69)
Contact atoms	29 (12)	30 (25)	32 (26)	47 (37)	37 (30)	43 (35)	58 (50)
Residence time, min	<1.4	<1.4	<1.4	14	57	1944	1626
Quotient*	<0.05	<0.05	<0.04	0.3 (0.4)	1.5 (1.9)	45.2(55.5)	28.0 (32.5)

*Calculated by dividing the residence time by the contact atoms.